Comput Geosci (2007) 11:235–248
DOI 10.1007/s10596-007-9048-8

ORIGINAL PAPER

The representer method for two-phase flow in porous media

John Baird · Clint Dawson

Received: 12 September 2006 / Accepted: 27 March 2007/ Published online: 24 May 2007

Abstract The representer method is applied to a one-dimensional two-phase flow model in porous media; capillary pressure and gravity are neglected. The Euler–Lagrange equations must be linearized, and one such linearization is presented here. The representer method is applied to the linear system iteratively until convergence, though a rigorous proof of convergence is out of reach. The linearization chosen is easy to calculate but does not converge for certain weights; however, a simple damping restores convergence at the cost of extra iterations. Numerical experiments are performed that illustrate the method, and quick comparison to the ensemble Kalman smoother is made.

Keywords Representer method · Two-phase flow · Porous media · Ensemble Kalman smoother

1 Introduction

In data assimilation, one typically seeks a solution that balances the model and observed data by minimizing a least-squares functional of model and measurement residuals. The representer method (RM) is one technique to solve the resulting Euler–Lagrange (E-L) system [5, 6]. The goal of this paper is to derive the RM for a nonlinear system in the subsurface. A quick comparison with the ensemble Kalman smoother serves to highlight the different issues one must overcome in applying these methods.

Underpinning the RM is the superposition principle for linear E-L systems. A linear, single-phase flow model has been examined by the authors [3]. However, realistic models of the subsurface include nonlinearities [4, 13]. The corresponding E-L systems are nonlinear and the superposition principle fails. To use the RM, one linearizes the E-L system and applies the method to the resulting system. Then, one iterates through a sequence of solutions to the linear systems to converge to the solution of the nonlinear system.

The goal is to find a linearization that converges, preferably in few iterations. The notion of convergence may be taken in several ways. Valstar [25] suggests that convergence is achieved when the difference between the values at the measurement locations of consecutive iterates is below some tolerance. One may consider convergence in terms of accuracy in computing a quantity of interest [2]. Here, the stopping criteria is based on the discrete L_1 norm in time and space of the difference of successive iterates. A rigorous proof of convergence is usually out of reach, but in practice one can often converge numerically.

In Section 2, a simple but useful nonlinear model is presented, and in Section 3, the RM for it is derived. More general weighting in the cost functional is assumed than for the previous work in the linear case to make a fair comparison to the Kalman smoother and to explore the effects of the correlation length on the quality of assimilation. A straightforward linearization of the E-L equations in which the coefficients are lagged is used; however, it does not always converge. A relatively simple fix akin to a line search or damping restores

This research was supported by NSF grant EIA-0121523.

J. Baird · C. Dawson (✉)
Center for Subsurface Modeling - C0200,
Institute for Computational Engineering and Sciences
(ICES), The University of Texas at Austin,
Austin, TX 78712, USA
e-mail: clint@ices.utexas.edu

convergence. The damping parameter has been found to be problem-dependent. For example, it depends on the choice of weights and the mesh size. The parameter is chosen through trial and error, though it would be desirable to have an automatic way of determining it.

In Section 4, the ensemble Kalman smoother is briefly presented and discussed. Then, in Section 5, some numerical experiments are described and performed. The RM is compared to the Kalman smoother in terms of implementation and computational difficulty and quality of solution.

2 Problem formulation

First, the model used for two-phase flow is presented. The two phases are water and oil, denoted by a subscript w and o, respectively. Saturation is denoted by S_α and flow velocity by u. K is the absolute permeability, κ_α is the relative permeability and μ_α is fluid viscosity. Gravity and capillary pressure are neglected, and the system is in one space dimension. Furthermore, incompressible flow is assumed. The following relationships and definitions hold:

$$S_\mathrm{w} + S_\mathrm{o} = 1, \quad P_\mathrm{o} = P_\mathrm{w}, \quad \lambda_\alpha = K\frac{\kappa_\alpha(S_\alpha)}{\mu_\alpha}, \quad \text{and} \quad \lambda_t = \lambda_\mathrm{w} + \lambda_\mathrm{o}. \tag{1}$$

Then, with appropriate boundary and initial conditions, the model equation is

$$\phi\frac{\partial S_{\mathrm{w},F}}{\partial t} + \frac{\partial}{\partial x} f(S_{\mathrm{w},F}) = F \quad \text{on } [0, L]\times(0, T] \tag{2}$$

$$S_{\mathrm{w},F}(x, 0) = I \quad \text{on } [0, L]\times\{0\} \tag{3}$$

$$S_{\mathrm{w},F}(0, t) = B \quad \text{on } \{0\}\times(0, T] \tag{4}$$

where $f(S_\mathrm{w}) = \frac{\lambda_\mathrm{w}}{\lambda_t}u$. Here, u is prescribed and is assumed to be positive. As an example of f, see Fig. 2. It is assumed that there are M measurements of the form

$$d_m = \mathcal{L}_m(\tilde{S}_\mathrm{w}) = \int_0^T\int_0^L H_m(x, t)\tilde{S}_\mathrm{w}(x, t)dxdt. \tag{5}$$

In the rest of the chapter, $S_{\mathrm{w},F}$ always refers to the solution to Eqs. 2–4, $\tilde{S}_\mathrm{w}$ refers to the "true" state in the system from which the measurements are taken, and $\hat{S}_\mathrm{w}$ is the updated or smoothed solution.

The system is overdetermined with the addition of the measurement data, barring the extremely unlikely case where the measured data are consistent. Therefore, residuals are defined via

$$\phi\frac{\partial S_\mathrm{w}}{\partial t} + \frac{\partial}{\partial x} f(S_\mathrm{w}) = F + f \quad \text{on } [0, L]\times(0, T] \tag{6}$$

$$S_\mathrm{w}(x, 0) = I + i \quad \text{on } [0, L]\times\{0\} \tag{7}$$

$$S_\mathrm{w}(0, t) = B + b \quad \text{on } \{0\}\times(0, T] \tag{8}$$

$$\mathbf{d} = \mathcal{L}(\tilde{S}_\mathrm{w}) = \mathcal{L}(S_\mathrm{w}) - \boldsymbol{\epsilon} \tag{9}$$

2.1 The E-L conditions

The notion of solution must now be redefined in terms of the residuals, and from the new definition, the RM is derived. Define the notation $\bullet$, $\circ$, and $*$ as integrations by

$$W_f \bullet f = \int_0^T\int_0^L W_f(x, t, y, s)\, f(x, t)dxdt \tag{10}$$

$$f \bullet W_f \bullet f = \int_0^T\int_0^L\int_0^T\int_0^L f(y, s)W_f(x, t, y, s) \times f(x, t)dxdtdyds \tag{11}$$

$$W_i \circ i = \int_0^L W_i(x, y)i(x)dx$$
$$i \circ W_i \circ i = \int_0^L\int_0^L i(y)W_i(x, y)i(x)dxdy \tag{12}$$

$$W_b * b = \int_0^T W_b(t, s)b(t)dt$$
$$b * W_b * b = \int_0^T\int_0^T b(s)W_b(t, s)b(t)dtds \tag{13}$$

The generalized inverse problem is to seek $\hat{S}_\mathrm{w}$, so that

$$J[\hat{S}_\mathrm{w}] = \min_{S_\mathrm{w}} J[S_\mathrm{w}] = \min_{S_\mathrm{w}}\left\{ f\bullet W_f\bullet f + i\circ W_i\circ i + b * W_b * b + \boldsymbol{\epsilon}^T\mathbf{w}\boldsymbol{\epsilon}\right\}. \tag{14}$$

The measurement weight $\mathbf{w}$ is a matrix in $\mathbb{R}^{M\times M}$.

Now, $f(S_w + \delta S_w) \approx f(S_w) + f'(S_w)\delta S_w$. Then

$$\frac{1}{2}\delta J[S_w] = \left(\phi\frac{\partial \delta S_w}{\partial t} + \frac{\partial}{\partial x}\left(f'(S_w)\delta S_w\right)\right) \bullet W_f \bullet \left(\phi\frac{\partial S_w}{\partial t} + \frac{\partial}{\partial x} f(S_w) - F\right) + \delta S_w(x,0) \circ W_i \circ \left(S_w(x,0) - I\right) + \delta S_w(0,t) * W_b * \left(S_w(0,t) - B\right) + \sum_{m=1}^{M}\sum_{n=1}^{M}(H_n \delta S_w) \bullet w_{mn} \bullet \epsilon_m \quad (15)$$

Let

$$\lambda = W_f \bullet \left(\phi\frac{\partial S_w}{\partial t} + \frac{\partial}{\partial x} f(S_w) - F\right). \quad (16)$$

Then, after integrating by parts, one obtains

$$\frac{1}{2}\delta J[S_w] = \int_0^L \left(\phi\lambda\delta S_w\big|_0^T\right)dx + \int_0^T \lambda f'(S_w)\delta S_w\big|_0^L dt - \int_0^T\int_0^L \left(\phi\frac{\partial\lambda}{\partial t} + f'(S_w)\frac{\partial\lambda}{\partial x}\right)\delta S_w dx dt + \int_0^L W_i \circ \left(S_w(x,0) - I\right)\delta S_w(x,0)dx + \int_0^T W_b * \left(S_w(0,t) - B\right)\delta S_w(0,t)dt + \int_0^T\int_0^L \sum_{m=1}^{M}\sum_{n=1}^{M} w_{mn} \bullet \left(\mathcal{L}_m(S_w) - d_m\right)H_n \delta S_w dx dt \quad (17)$$

Now, in order for δJ to equal zero, the coefficients of δS_w must be zero. The formal inverse of the weights are defined via the relationships $C_f \bullet W_f = \delta(x-y)\delta(t-s)$, $C_i \circ W_i = \delta(x-y)$, $C_b * W_b = \delta(t-s)$, $\mathbf{C}_\epsilon \mathbf{w} = \mathbf{I}$. The weights are assumed to be symmetric and positive definite. Then, one can write the E-L equations for the minimizer $\hat{S}_w$ and multiplier $\hat{\lambda}$ as follows. Note that Eq. 21 is the definition of $\hat{\lambda}$:

$$-\phi\frac{\partial\hat{\lambda}}{\partial t} - f'\left(\hat{S}_w\right)\frac{\partial\hat{\lambda}}{\partial x} = -\sum_{m=1}^{M}\sum_{n=1}^{M} w_{mn}\left(\mathcal{L}_m(\hat{S}_w) - d_m\right)H_n \quad \text{on } [0,L]\times[0,T) \quad (18)$$

$$\phi\hat{\lambda} = 0 \quad \text{on } [0,L]\times\{T\} \quad (19)$$

$$\hat{\lambda} f'\left(\hat{S}_w\right) = 0 \quad \text{on } \{L\}\times[0,T) \quad (20)$$

$$\phi\frac{\partial\hat{S}_w}{\partial t} + \frac{\partial}{\partial x} f\left(\hat{S}_w\right) = F + C_f \bullet \hat{\lambda} \quad \text{on } [0,L]\times(0,T] \quad (21)$$

$$\hat{S}_w = I + C_i \circ \phi\hat{\lambda} \quad \text{on } [0,L]\times\{0\} \quad (22)$$

$$\hat{S}_w = B + C_b * \hat{\lambda} f'\left(\hat{S}_w\right) \quad \text{on } \{0\}\times(0,T] \quad (23)$$

One cannot first solve for $\hat{\lambda}$ and then solve for $\hat{S}_w$ because $\hat{S}_w$ appears in the forcing for Eq. 18. However, there is a further complication in that the coefficients of the partial differential equation for $\hat{\lambda}$ involve $\hat{S_w}$ and the adjoint equation is of a slightly different form than the forward equation.

3 The representer method

The main difficulty in applying the RM to this system is that it is not linear. Thus, the superposition principle does not hold. One way of overcoming this obstacle is to linearize the system and iterate. Consider the following linearized scheme: Let $\hat{S}_w^0$ be the solution to the forward model Eqs. 2–4. Then, let $\hat{S}_w^k$ be given by

$$-\phi\frac{\partial\hat{\lambda}^k}{\partial t} - f'\left(\hat{S}_w^{k-1}\right)\frac{\partial\hat{\lambda}^k}{\partial x} = -\sum_{m=1}^{M}\sum_{n=1}^{M} w_{mn}\left(\mathcal{L}_m\left(\hat{S}_w^k\right) - d_m\right)H_n \quad \text{on } [0,L]\times[0,T) \quad (24)$$

$$\phi\hat{\lambda}^k = 0 \quad \text{on } [0,L]\times\{T\} \quad (25)$$

$$\hat{\lambda}^k f'\left(\hat{S}_w^{k-1}\right) = 0 \quad \text{on}\{L\}\times[0,T) \quad (26)$$

$$\phi\frac{\partial\hat{S}_w^k}{\partial t} + f'\left(\hat{S}_w^{k-1}\right)\frac{\partial\hat{S}_w^k}{\partial x} = F + C_f \bullet \hat{\lambda}^k \quad \text{on } [0,L]\times(0,T] \quad (27)$$

$$\hat{S}_w^k = I + C_i \circ \phi\hat{\lambda}^k \quad \text{on } [0,L]\times\{0\} \quad (28)$$

$$\hat{S}_w^k = B + C_b * \hat{\lambda}^k f'\left(\hat{S}_w^{k-1}\right) \quad \text{on } \{0\}\times(0,T] \quad (29)$$

Now the RM can be used to solve the system at each iteration. One assumes

$$\hat{S}_{\mathrm{w}}^k = S_{\mathrm{w},F} + S_c^k + \sum_{m=1}^{M} \beta_m^k r_m^k. \tag{30}$$

The definition of r_m^k is

$$-\phi \frac{\partial \alpha_m^k}{\partial t} - f'\left(\hat{S}_{\mathrm{w}}^{k-1}\right) \frac{\partial \alpha_m^k}{\partial x} = H_m \quad \text{on } [0, L]\times[0, T) \tag{31}$$

$$\phi \alpha_m^k = 0 \qquad \text{on } [0, L] \times \{T\} \tag{32}$$

$$\alpha_m^k f'\left(\hat{S}_{\mathrm{w}}^{k-1}\right) = 0 \qquad \text{on } \{L\} \times [0, T) \tag{33}$$

$$\phi \frac{\partial r_m^k}{\partial t} + f'\left(\hat{S}_{\mathrm{w}}^{k-1}\right) \frac{\partial r_m^k}{\partial x} = C_f \bullet \alpha_m^k \quad \text{on } [0, L]\times(0, T] \tag{34}$$

$$r_m^k = C_i \circ \phi \alpha_m^k \qquad \text{on } [0, L] \times \{0\} \tag{35}$$

$$r_m^k = C_b * \alpha_m^k f'\left(\hat{S}_{\mathrm{w}}^{k-1}\right) \qquad \text{on } \{0\} \times (0, T] \tag{36}$$

The correction term S_c^k is needed to account for the linearization and is defined so that

$$\phi \frac{\partial}{\partial t}\left(S_{\mathrm{w},F} + S_c^k\right) + f'\left(\hat{S}_{\mathrm{w}}^{k-1}\right) \frac{\partial}{\partial x}\left(S_{\mathrm{w},F} + S_c^k\right) = F \quad \text{on } [0, L] \times (0, T] \tag{37}$$

$$\left(S_{\mathrm{w},F} + S_c^k\right)(x, 0) = I \qquad \text{on } [0, L] \times \{0\} \tag{38}$$

$$\left(S_{\mathrm{w},F} + S_c^k\right)(0, t) = B \qquad \text{on } \{0\} \times (0, T] \tag{39}$$

To see that the correction term is needed, it is necessary to go through the derivation for β_m^k. By applying the linearized equation to the expansion of $\hat{S}_{\mathrm{w}}^k$, Eq. 30, and using the definitions of $S_{\mathrm{w},F}$, S_c^k Eq. 37, and r_m^k Eq. 34, one obtains:

$$\begin{aligned}\mathcal{D}\hat{S}_{\mathrm{w}}^k &= \mathcal{D}\left(S_{\mathrm{w},F} + S_c^k\right) + \sum_{m=1}^{M} \beta_m^k \mathcal{D} r_m^k \\ &= F + \sum_{m=1}^{M} \beta_m^k C_f \bullet \alpha_m^k\end{aligned} \tag{40}$$

where $\mathcal{D}S = \phi \frac{\partial S}{\partial t} + f'(\hat{S}_{\mathrm{w}}^{k-1}) \frac{\partial S}{\partial x}$. Recall that W_f is the inverse of C_f and use the last expression and the definition of λ^k Eq. 27 to obtain

$$\sum_{m=1}^{M} \beta_m^k \alpha_m = W_f \bullet \left(\mathcal{D}\hat{S}_{\mathrm{w}}^k - F\right) = \lambda^k. \tag{41}$$

Furthermore, combining Eqs. 24 and 31 with Eq. 41, one sees that

$$\begin{aligned}&-\sum_{m=1}^{M}\sum_{n=1}^{M} w_{mn}\left(\mathcal{L}_m\left(\hat{S}_{\mathrm{w}}^k\right) - d_m\right) H_n \\ &\quad = \mathcal{D}^*\lambda^k = \sum_{n=1}^{M} \beta_n^k \mathcal{D}^* \alpha_n^k = \sum_{n=1}^{M} \beta_n^k H_n\end{aligned} \tag{42}$$

where $\mathcal{D}^* S = -\phi \frac{\partial S}{\partial t} - f'\left(\hat{S}_{\mathrm{w}}^{k-1}\right) \frac{\partial S}{\partial x}$.

Therefore, $\beta_n^k = -\sum_{m=1}^{M} w_{mn}\left(\mathcal{L}_m\left(\hat{S}_{\mathrm{w}}^k\right) - d_m\right)$. One cannot find $\mathcal{L}_m\left(\hat{S}_{\mathrm{w}}^k\right)$ without β_m^k, so a substitution yields

$$\beta_n^k = -\sum_{m=1}^{M} w_{mn}\left(\mathcal{L}_m\left(S_{\mathrm{w},F} + S_c^k\right) + \sum_{l=1}^{M} \beta_l \mathcal{L}_m\left(r_l^k\right) - d_m\right). \tag{43}$$

In matrix-vector notation, this is the system

$$\beta^k = -\mathbf{w}\left(\boldsymbol{\mathcal{L}}\left(S_{\mathrm{w},F} + S_c^k\right) + \mathbf{R}^k \boldsymbol{\beta}^k - \mathbf{d}\right). \tag{44}$$

$$\left(\mathbf{R}^k + \mathbf{C}_\epsilon\right)\boldsymbol{\beta}^k = \mathbf{d} - \boldsymbol{\mathcal{L}}\left(S_{\mathrm{w},F} + S_c^k\right) \tag{45}$$

where the entries of the matrix $\mathbf{R}^k$ are $r_{ml}^k = \mathcal{L}_m\left(r_l^k\right)$, and $\mathbf{C}_\epsilon \mathbf{w} = \mathbf{I}$.

Figure 1 is a flowchart that summarizes the RM applied to this problem.

3.1 Modifications

One can update the solution via Eq. 30 or 27. $\left(\hat{\lambda}^k = \sum \beta_m^k \alpha_m^k.\right)$ However, in this nonlinear case, there

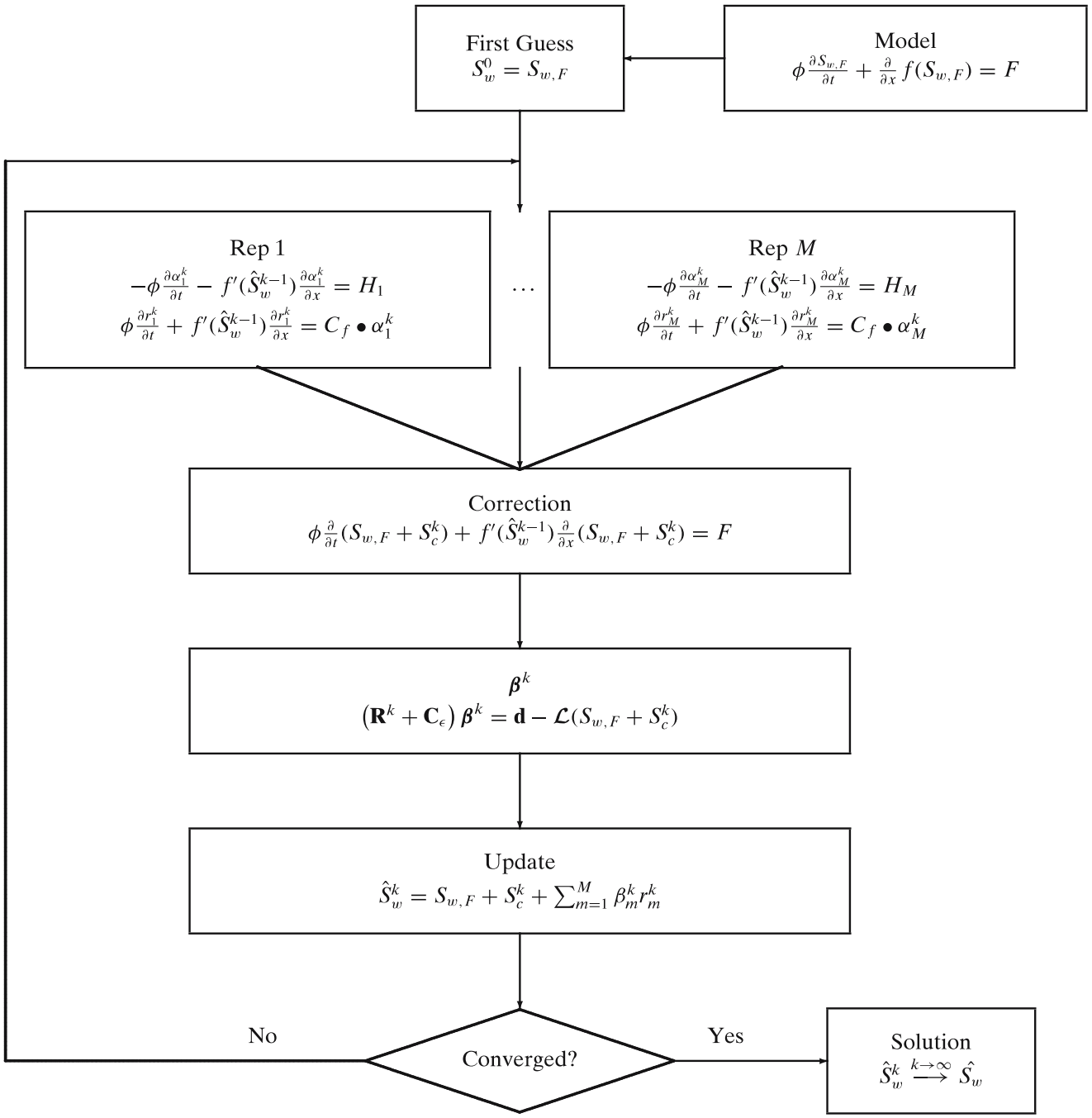

Fig. 1 Flowchart of the RM applied to a nonlinear problem. Note that this is assuming the update is Eq. 30 and not the alternatives discussed in Section 3.1. Also, the damping term θ, explained in the same section, is not included here

is a third option, one that is particularly attractive. For each iteration, the representers and β are computed as normal via Eqs. 31–36 and 45. Then, one returns to the nonlinear equation, Eq. 21, to update the state. Numerical experience shows that implementing this third option can dramatically improve convergence and captures the nonlinear front behavior better, in so far as a lag in the front speed seen when computing via Eq. 30 or 27 is corrected. Furthermore, when computing in this way, the effect of the correction term is negligible. An example is shown in Section 5, see, in particular, Figs. 5 and 4.

The linearization shown did not always converge, depending on the choice of weights. However, dampening each iterate in the following sense restored convergence: first calculate $\hat{S}_w^k$ via one of the previously

mentioned methods, then replace as in $\hat{S}_{\mathrm{w}}^{k} \leftarrow \theta \hat{S}_{\mathrm{w}}^{k} + (1-\theta)\hat{S}_{\mathrm{w}}^{k-1}$. Thus, the update is now defined as

$$\hat{S}_{\mathrm{w}}^{k} = \theta \left(S_{\mathrm{w},F} + S_{c}^{k} + \sum_{m=1}^{M} \beta_{m}^{k} r_{m}^{k} \right) + (1-\theta)\hat{S}_{\mathrm{w}}^{k-1}. \tag{46}$$

Note that taking $\theta = 1$ recovers the original method. Smaller θ usually means more iterations, while choosing θ too large may lose convergence. Thus, it is important to choose the largest possible θ for which convergence is achieved. In this work, θ was picked via trial and error. This method has been applied in this context by Valstar [25], and is also well known in the iterative solver community.

4 The ensemble Kalman smoother

The Kalman smoother is often thought of in terms of a prediction and correction pairing. One begins by creating an ensemble of model predictions of size N, here indexed by $i = 1, 2, ..., N$. Each model prediction satisfies

$$\phi \frac{\partial S_{\mathrm{w}}^{i}}{\partial t} + \frac{\partial}{\partial x} f(S_{\mathrm{w}}^{i}) = F + f_{i} \tag{47}$$

$$S_{\mathrm{w}}^{i}(x, 0) = I + i_{i} \tag{48}$$

$$S_{\mathrm{w}}^{i}(0, t) = B + b_{i} \tag{49}$$

Here, f_i, i_i, and b_i are random fields with covariances C_f, C_i, and C_b, respectively. Also, one creates an ensemble of measurements [7] via

$$\mathbf{d}_{i} = \mathbf{d} + \boldsymbol{\epsilon}_{i} \in \mathbb{R}^{M} \tag{50}$$

where M is the number of measurements and $\boldsymbol{\epsilon}_i$ is a vector whose components are drawn to have covariance $\mathbf{C}_\epsilon$. Let $D = (\mathbf{d}_i) \in \mathbb{R}^{M\times N}$ be the matrix containing these measurements and $Y = (\boldsymbol{\epsilon}_i) \in \mathbb{R}^{M\times N}$ be the matrix containing the perturbations.

The correction step is to perform the update at all times prior to the measurement time via the Kalman gain. For times after the measurement, the model is used. In this paper, there will only be one measurement time, and so no account is taken of the cycling nature of the Kalman smoother.

One uses the ensemble just constructed to approximate the covariances of the system. In this way, the EnKS is to able bypass the need for computing an adjoint, which can be a considerable advantage in terms of the time it takes to implement an adjoint. For a derivation of the equations and the method that the authors use for calculations, see Evensen [11], particularly Appendix D. The equations are presented in a finite-dimensional setting, so let Nx represent the size of the mesh discretization in space. Let $A(t') = (S_{\mathrm{w}}^{i}(t')) \in \mathbb{R}^{\mathrm{Nx}\times N}$ be the matrix of ensemble members at time $t' < t$, where t is the measurement time. Then let $A'(t') = A(t') - \bar{A}(t')$, where $\bar{A}(t')$ is the matrix where each column is the average of the ensemble. Let $\boldsymbol{\mathcal{L}}(A') \in \mathbb{R}^{M\times N}$ be the matrix whose columns are the measurements of A'; in Evensen's notation $\boldsymbol{\mathcal{L}}(A') = HA'(t)$. One can write the update as $A^a \in \mathbb{R}^{\mathrm{Nx}\times N}$, where

$$A^{a}(t') = A(t') + A'(t')\boldsymbol{\mathcal{L}}(A')^{T} \times \left(\boldsymbol{\mathcal{L}}(A')\boldsymbol{\mathcal{L}}(A')^{T} + YY^{T}\right)^{-1} (D - \boldsymbol{\mathcal{L}}(A)). \tag{51}$$

For comparison with the RM, the EnKS solution is considered to be the average of the updated ensemble.

It is especially important to choose reasonable covariances in order for the ensemble Kalman smoother to work. If the covariances are large, then saturation values may be chosen that are unphysical, for instance, below the residual saturation.

Additionally, the mesh and time step sizes should be smaller than the correlation length of the covariances to avoid filtering effects. Ababou and coauthors suggest at least five grid points within a correlation length [1]. To this end, a noise model presented by Evensen [11] is adopted whereby correlated noise is computed from white noise. Let w_k be a sequence of numbers from $\mathcal{N}(0, 1)$. Then, the sequence q_k given by

$$q_{k} = q_{k-1} + \sqrt{1-\alpha^{2}}\, w_{k-1} \tag{52}$$

has covariance $\overline{q_i q_j} = \alpha^{|i-j|}$. The correlation length is determined by the choice of α, which in turn depends on the mesh or time step size. Evensen suggests choosing $\tau > \Delta t$ and then $\alpha = 1 - \Delta t/\tau$. In Section 5.2.1, this noise model is used for the boundary condition in example 1, that is, q_k becomes b_i in Eq. 49.

There are two other reasons to use correlated noise. Firstly, one usually expects errors to be correlated on physical grounds. Secondly, the more correlated the noise, the smaller the ensemble needs to be to fully capture the behavior of the system. If pure white noise is added at each time step, then the ensemble size is dependent on the size or number of the time steps.

4.1 Comparison to the representer method

The EnKS solves the same minimization problem as the RM in a single cycle; that is to say it also finds the minimum of Eq. 14. Therefore, the two methods give the same state update assuming both methods are fully converged (number of ensemble members for EnKS and iterations for RM), the model and measurements are linear, the covariances are normal with zero mean,

and EnKS is not performed for more than one cycle. For further discussion and proof, see Bennett [6]. When the model is nonlinear, as is the case here, there are differences, and these are discussed in the results section for example 1, Section 5.3. In particular, the mean of the updated states in the EnKS is the best estimate of the state in the linear case, but in the nonlinear case, one sees that taking such an average results in an state that has a nonphysical, smeared front.

It is also important to compare the computational work required by EnKS and the RM. An advantage that both methods enjoy is that the representers and the ensemble members can be calculated independently. Thus, both methods lend themselves to parallelization.

An estimate for the EnKS is that, for moderately sized problems, 100 to 500 ensemble members are sufficient [22]. However, this number depends on the nonlinearity and varies from application to application; the authors know of no rigorous bounds on the number of members needed. In this paper, 500 ensemble members are used, as the results for example 1, see Section 5.3, then do not change as more members are added.

The work required for the RM, on the other hand, increases with the number of measurements and the number of iterations required to converge. The number of iterations depends on the nonlinearity and is problem-dependent. Thus, for M measurements and N_i iterations, one needs MN_i adjoint solves and $(M+1)N_i+1$ forward solves. The correction term computations are ignored, as their effect is negligible, at least for these problems. In example 1, 35 iterations are needed and one measurement is used for a total of 106 integrations. For this problem, assuming all else stays equal, the RM would require more integrations than the EnKS for seven or more measurements.

Bennett suggests strategies to deal with large numbers of measurements, including analyzing the measurement array with the representers to identify and remove unneeded measurements [6]. The authors have also previously explored ways of computing the representers on coarser grids [2].

5 Numerical experiments

5.1 Discretizations

For the nonlinear model, a Godunov method is used [8, 14, 16]. The Godunov flux function G is given by

$$G(S_l, S_r) = \begin{cases} \min\limits_{S_l \le S \le S_r} f(S) & \text{if } S_l \le S_r \\ \max\limits_{S_r \le S \le S_l} f(S) & \text{if } S_l > S_r \end{cases} \tag{53}$$

In the case where the flux f is monotonically increasing, the flux function simplifies to $G(S_l, S_r) = S_l$. For the linear models, both adjoint and forward, one-sided methods are used, where $A^{k,n}_{i,i-1} = 0.5\left(f'\left(\hat{S}^{k-1,n}_{\mathrm{w},i}\right) + f'\left(\hat{S}^{k-1,n}_{\mathrm{w},i-1}\right)\right)$.

For all the methods, Euler time stepping is implemented. To satisfy the Courant–Friedrichs–Lewy condition for the linear models, one must choose Δt so that

$$\frac{\Delta t}{\Delta x}\left(\max_{S\in[S_{wr},\,1-S_{or}]} f'(S)\right) \le 1. \tag{54}$$

5.1.1 Forward model

$$S^{n+1}_{\mathrm{w},i} = S^n_{\mathrm{w},i} + \frac{\Delta t}{\phi} \times\left(-\frac{G\left(S^n_{\mathrm{w},i}, S^n_{\mathrm{w},i+1}\right) - G\left(S^n_{\mathrm{w},i-1}, S^n_{\mathrm{w},i}\right)}{\Delta x} + F\left(x_i, t^n\right)\right) \tag{55}$$

5.1.2 Adjoint

$$\alpha^{k,n-1}_{m,i} = \alpha^{k,n}_{m,i} + \frac{\Delta t}{\phi}\left(A^{k,n}_{i+1,i}\frac{\alpha^{k,n}_{m,i+1} - \alpha^{k,n}_{m,i}}{\Delta x} - H_m\left(x_i, t^n\right)\right) \tag{56}$$

5.1.3 Representer

$$r^{k,n+1}_{m,i} = r^{k,n}_{m,i} + \frac{\Delta t}{\phi}\left(-A^{k,n}_{i,i-1}\frac{r^{k,n}_{m,i} - r^{k,n}_{m,i-1}}{\Delta x} + \left(C_f \bullet \alpha^k\right)^n_{m,i}\right) \tag{57}$$

5.1.4 Correction

$$S^{k,n+1}_{c,i} = S^{k,n}_{c,i} + \frac{\Delta t}{\phi}\left(-A^{k,n}_{i,i-1}\frac{S^{k,n}_{c,i} - S^{k,n}_{c,i-1}}{\Delta x}\right) + \frac{\Delta t}{\phi}\left(F\left(x_i, t^n\right) - \left(\phi\frac{S^{n+1}_{\mathrm{w},i} - S^n_{\mathrm{w},i}}{\Delta t} + A^{k,n}_{i,i-1}\frac{S^n_{\mathrm{w},i} - S^n_{\mathrm{w},i-1}}{\Delta x}\right)\right) \tag{58}$$

5.2 Descriptions of examples

5.2.1 Example 1

The first example is chosen to be relatively simple for clarity and to illustrate the various difficulties

one encounters. The following parameters are chosen: $L = 1$, $T = 1$, $S_{wr} = .25$, $S_{or} = .15$, $K = 1$, $u = 0.4$, $\mu_w = 1$, $\mu_o = 10$, $\phi = 0.45$, and

$$\kappa_w = 0.4\left(\frac{Sw - 0.25}{0.6}\right)^{4.2} \qquad \kappa_o = 0.9\left(\frac{0.85 - Sw}{0.6}\right)^{1.2} \tag{59}$$

Figure 2 shows $\lambda_w(S_w)$ and $\lambda_o(S_w)$ and f and its derivative.

The "true" solution from which the measurements are drawn, $\tilde{S}_w$, is the forward model solution with initial condition $I = S_{wr}$, $F = 0$, and $B = 0.77$. The model solution, $S_{w,F}$, has error only in the boundary condition and uses $B = 0.65$ instead; all else is the same. All solutions were computed with the discretization $\Delta x = 100^{-1}$ and $\Delta t = 500^{-1}$.

Only one measurement is used for this first example. The measurement is the average saturation at $t = 0.5T$ from $x = 0.25$ to $x = 0.5$. The inverse weights for the forcing and initial condition are zero, $C_f = 0$ and $C_i = 0$.

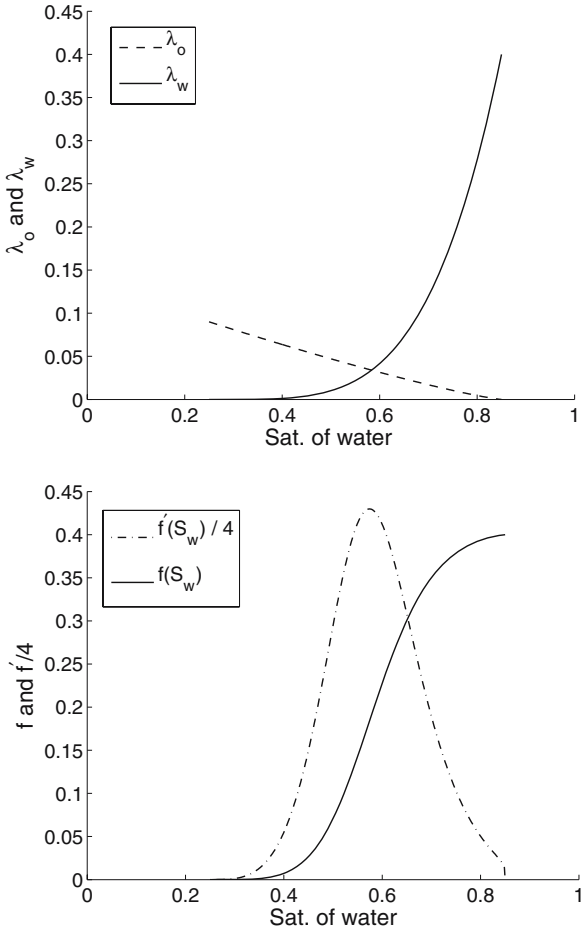

Fig. 2 *Left*: $\lambda_w(S_w)$ and $\lambda_o(S_w)$ *Right*: $f(S_w)$ and $f'(S_w)$

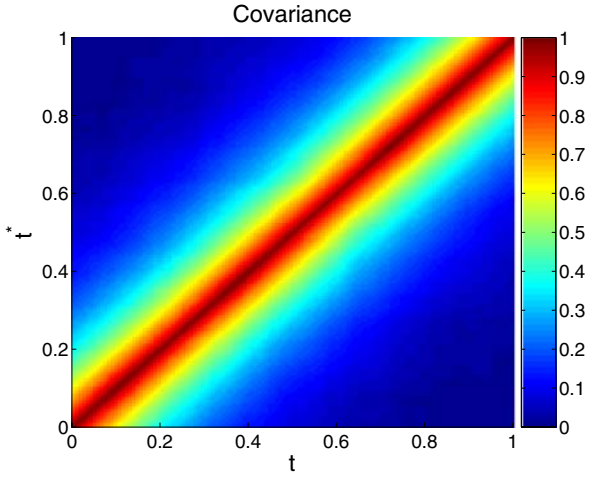

Fig. 3 C_b scaled by 1/0.01

The measurement variance is the scalar $C_\epsilon = 0.01$. The weight for the boundary is a bit more complex. To make a fair comparison with the Kalman smoother, it is necessary to use a covariance with a correlation length larger than the grid size. This precludes a constant weight. Recalling that the inverse weight is a covariance, the noise model in Eq. 52 is used with $\tau = 0.2$, see Fig. 3. The covariance is then multiplied by 0.01 to be used as C_b.

5.2.2 Example 2

In the second example, the ability of the RM to adjust for heterogeneity is tested. All the same parameters as in the first example are used, except that $L = 0.5$ and the porosity is varied. For the truth, $\tilde{S}_w$, ϕ is given by

$$\phi = \begin{cases} 0.60 & \text{if } 0 \le x < 0.25 \\ 0.45 & \text{if } 0.25 \le x < 0.5 \\ 0.82 & \text{if } 0.5 \le x < 0.75 \\ 0.42 & \text{if } 0.75 \le x \le 1 \end{cases} \tag{60}$$

The initial and boundary conditions for both the truth and model are $I = 0.45$ and $B = 0.55$. The forcing is $F = 0$. The model solution is computed with a constant porosity of $\phi = 0.46$. All solutions were computed with the discretization $\Delta x = 100^{-1}$ and $\Delta t = 1000^{-1}$.

For this example, five measurements are taken of the average saturation of water. The average is taken at the points $x = 0.1$, $x = 0.2$, $x = 0.3$, $x = 0.4$, and $x = 0.5$ over the time interval $t \in [.6, 1]$.

5.3 Results

Part of this example illustrates the effect of the form of the weights on the assimilated solution. Suppose

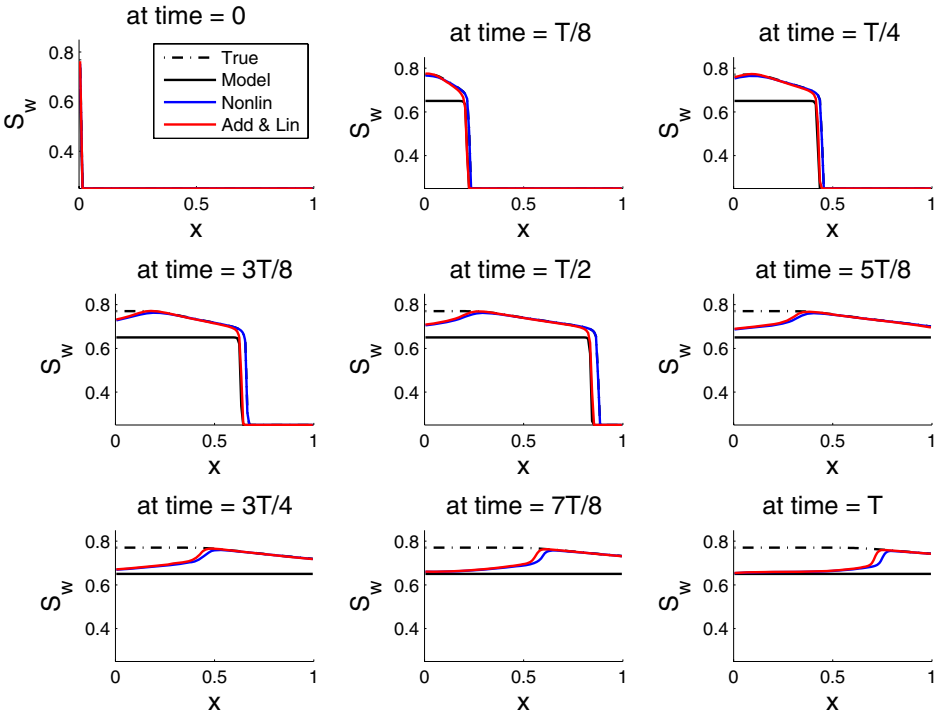

Fig. 4 Comparison of solution methods: "Add," "lin," and "nonlin"

that one has some reason to suspect that the error is indeed caused by a misspecification of porosity. Then, one ought to extend the methodology to a full parameter estimation RM as discussed in the conclusions. However, it is shown here that one can improve the state assimilation by encoding that information into the covariances. Thus, three different correlations are used. The weights and their effects are described in the results section.

5.3.1 Example 1

To begin, the three different ways of computing the RM mentioned at the end of Section 3 are compared. These are referred to as "nonlin" Eq. 21, "lin" Eq. 27, and "add" Eq. 30. Of course, in all three cases the representers are computed via Eqs. 31–36. The scheme is considered to have converged when two consecutive iterates differ by less than 10^{-6} in the L_1-norm in time and space. To obtain convergence, $\theta = 0.35$ was used.

In this example, "add" and "lin" agreed to machine precision. Figure 4 shows all three smoothed solutions together with the true and model solutions. Though all three lie nearly on top of each other, there is an important difference. Namely, the front of "add" and "lin" move at the speed of the model, which is incorrect for that saturation from a physical standpoint. The front speed of "nonlin" agrees with the true solution and is physically correct. Not only is "nonlin" physically superior, but it also has better convergence properties as evidenced by Fig. 5.

Figure 6 sheds light on the physics of the problem by showing a dimensionless plot of the true, model, and assimilated solutions. The dimensionless parameters are $x_D = x/L$ and $t_D = (ut)/(\phi L)$. The black line represents the location of the measurement. One can see how the model is improved along the characteristics that flow into and out of the measurement. The representers, computed via the adjoint, capture this information.

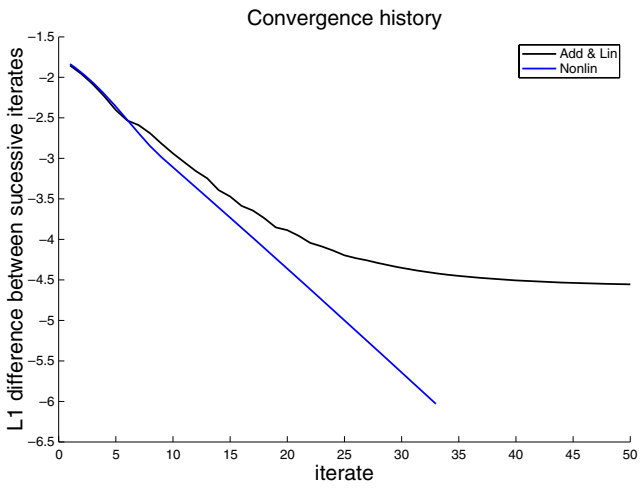

Fig. 5 Convergence history for the three solution methods. The ordinate axis is on a base 10 logarithmic scale

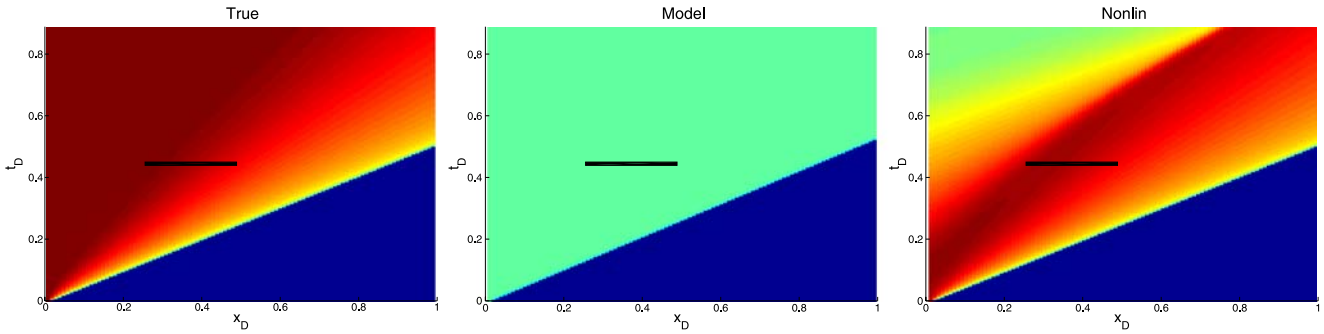

Fig. 6 Dimensionless plots of solutions

The ensemble Kalman smoother was also used to solve this problem, with 500 ensemble members. About 500 ensembles were needed for the results to be independent of the ensemble size, in that more members did not change the result in the discreet L_1 norm in space and time by more than 10^{-6}. To compare the amount of work performed, the "nonlin" representer solution required about 35 iterations to converge so that about 106 model and adjoint integrations were needed. Of course, the number of integrations for the RM grows with the number of measurements, which is not the case for the Kalman smoother.

The first thing to notice about the EnKS solution is that the front is severely and nonphysically smoothed. The cause of the smoothing is that the front behavior is nonlinear; therefore, though each ensemble member has a sharp front, the mean does not. Figure 7 shows a time snapshot of the solution and the ensemble members, with the model subtracted out for clarity. This suggests that the mean is not the best quantity to study. For this particular problem, one is able to fix this shortcoming at the cost of only one extra integration.

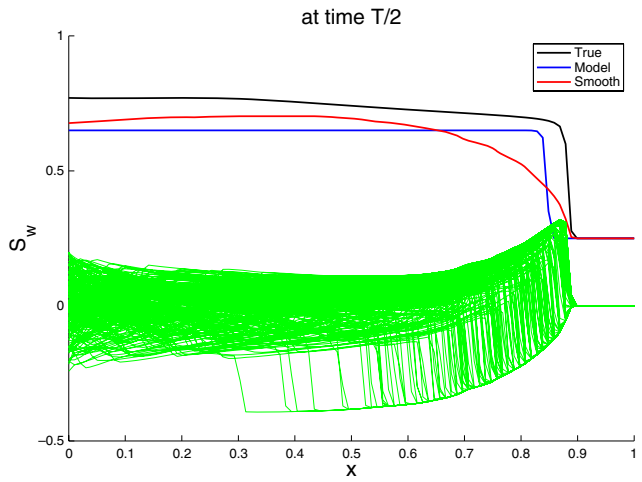

Fig. 7 Snapshot of the ensemble and analysis at $t = 0.5$. The green lines are ensemble members subtracted by the model so they are distinguishable from the EnKS analysis

This fix is labeled "mEnKS" and is obtained by computing the Kalman solution, "EnKS," and then, as there are only errors in the boundary data, taking the smoothed boundary as forcing and running the model. Both solutions are shown in Fig. 8. Figure 9 shows the dimensionless plots.

Though the EnKS solution is physically incorrect, with the fix, it produces a solution that is much better than the forward model and is shaped similarly to the RM. However, neither solution corrects as well as the representer solution, especially near the measurement.

On a further note, the EnKS is sensitive to the size of the weights as discussed earlier. A large covariance makes it likely that unphysical saturations are picked as model forcings. The representer is more robust in this sense, in that it is able to handle nearly any choice of weight.

Table 1 contains a comparison of the quality of the assimilations performed, both at the measurements and in a more global sense. It is clear that the RM outperforms the ensemble Kalman smoother in this example. Note that the poor front behavior of EnKS causes there to be little improvement in the global error measure.

5.3.2 Example 2

This example illustrates that one can improve the estimate of the state by encoding information in the covariances. It also illustrates the limitations of a data assimilation method that is limited to state estimation, as the following covariances are picked basically through trial and error. A more theoretically sound approach is the full parameter and state estimation problem, mentioned in the conclusions as the natural next step.

Figure 10 shows the true, model, and smoothed solutions for three different choices of weights (and, thus, covariances). All three solutions use $C_i = 0$, $C_b = 0$, and $\mathbf{C}_\epsilon = 0.00075\mathbf{I}$.

The first smoothed solution, labeled "Nonlin 1," corresponds to perfect decorrelation in time and space,

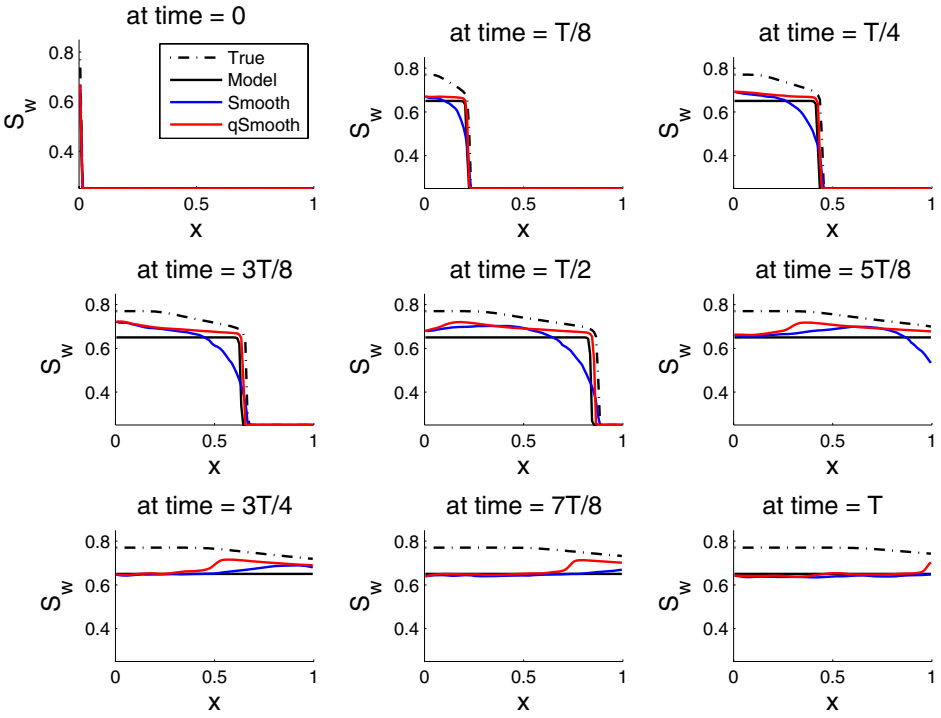

Fig. 8 The ensemble Kalman smoother

and the covariance is $C_f = 0.25\delta(x-y)\delta(t-s)$. Notice that the correction to the model is localized in time and, furthermore, strictly follows the characteristics. The RM is not picking up on the systematic bias. Adding many more measurements at different times may improve the situation, but one would need a dense measurement array. Or, one may try to encode more information in the covariance. For the second solution, labeled "Nonlin 2," C_f is taken to be perfectly correlated in time because the porosity is constant in time. C_f is taken to be $C_f = 0.25\delta(x-y)$. One can see an improvement during the time of the measurements that matches the pattern of the porosity; however, there is a dramatic undershoot in the assimilation at earlier times before the front moves through.

This suggests a perfect correlation in time is also not appropriate. One needs further study of the term that gives rise to the error. Because of the model formulation, the effect of errors in porosity depends upon the saturations themselves. If $\tilde{\phi}$ is the true porosity and ϕ_e is the error, one can write the model as

$$\tilde{\phi}\frac{\partial S_{\mathrm{w},F}}{\partial t} + \frac{\partial}{\partial x} f\left(S_{\mathrm{w},F}\right) = F - \phi_e \frac{\partial S_{\mathrm{w},F}}{\partial t}. \tag{61}$$

The term on the right-hand side is then the model residual f. So, the porosity error is multiplied by the time derivative $S_{\mathrm{w},F}$. One would expect then that the covariance structure should depend on the $S_{\mathrm{w},F}$. Because the time derivative of $S_{\mathrm{w},F}$ is most significant at the front, one way to incorporate this information is to split the correlation in time into two regimes, before and after the front.

Thus, for the third try, the covariance was taken to be $C_f = 0.048\delta(x-y)$ before the front and $C_f =$

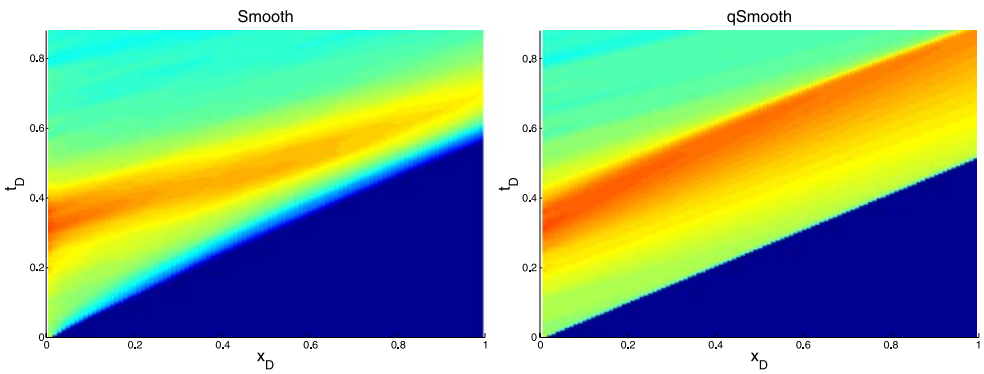

Fig. 9 Dimensionless plots of solutions for the Kalman smoother. "EnKS" refers to the traditional EnKS. "mEnKS" is the fix of the oversmoothing that is applicable only to this particular problem

Table 1 Measures of assimilation quality

	$\|\mathcal{L}(S_{w,F}) - \mathbf{d}\|_2$	$\|S_{w,F} - \tilde{S}_w\|_{L^2(0,T;L^2(\Omega))}$
Model	1.124e-1	7.724e-2
	$\|\mathcal{L}(\hat{S}_w) - \mathbf{d}\|_2$	$\|\hat{S}_w - \tilde{S}_w\|_{L^2(0,T;L^2(\Omega))}$
Add & Lin	4.486e-4	2.621e-2
Nonlin	3.932e-3	2.222e-2
EnKS	5.920e-2	7.245e-2
mEnKS	5.829e-2	5.419e-2

Table 2 Measures of assimilation quality

	$\|\mathcal{L}(S_{w,F}) - \mathbf{d}\|_2$	$\|S_{w,F} - \tilde{S}_w\|_{L^2(0,T;L^2(\Omega))}$
Model	5.390e-2	1.029e-2
	$\|\mathcal{L}(\hat{S}_w) - \mathbf{d}\|_2$	$\|\hat{S}_w - \tilde{S}_w\|_{L^2(0,T;L^2(\Omega))}$
Nonlin 1	1.159e-3	1.024e-2
Nonlin 2	2.271e-2	7.047e-3
Nonlin 3	2.285e-2	6.614e-3

$0.26\delta(x-y)$ after the front has passed. The measurements are taken after the front and so the correlation there is higher. The last solution, labeled "Nonlin 3," is the result. Note that, after the front, the solution is corrected similarly to "Nonlin2," but the severe undershoot has been corrected.

Table 2 contains some measures of the quality of the assimilation. One can see that, in all cases, the assimilated solution more closely matches the true solution than the model, both at the measurement sites and in a global sense. However, note the trade-off between accuracy at the measurements and global accuracy.

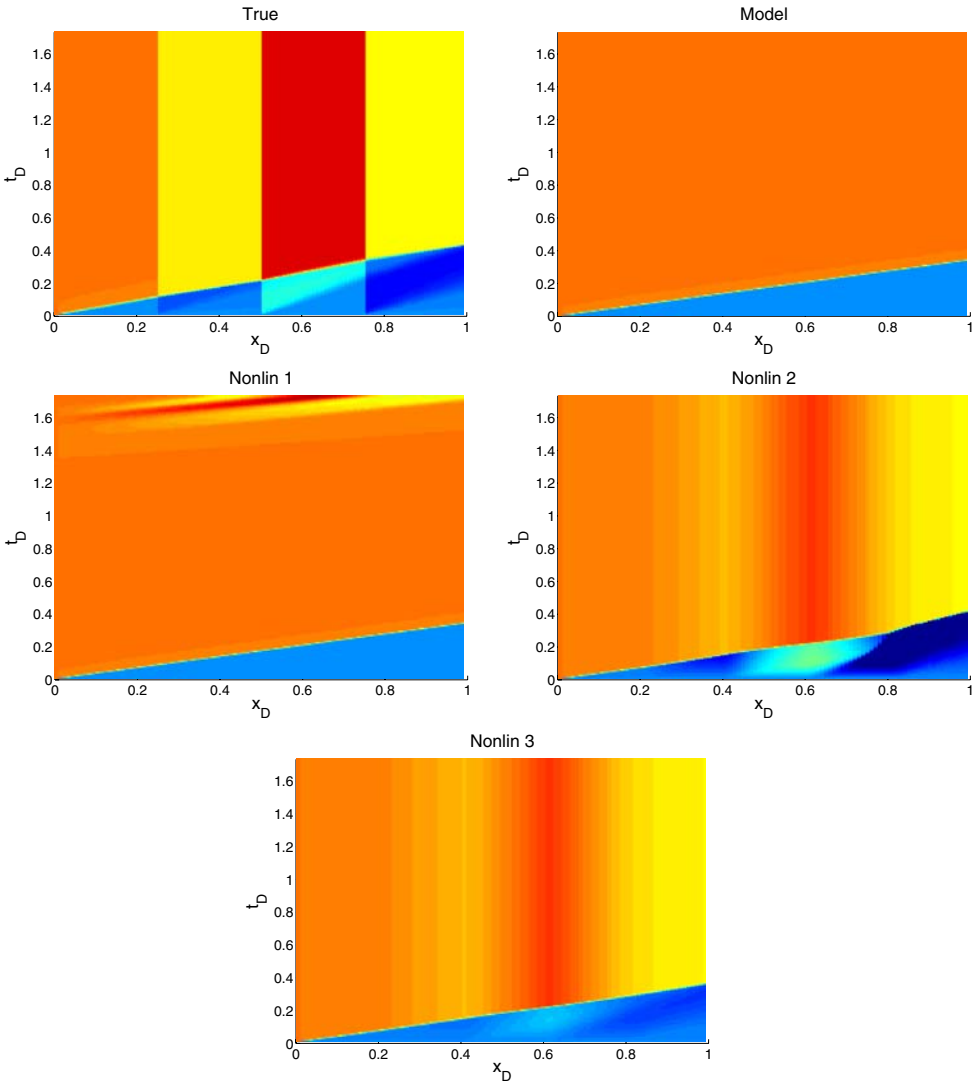

Fig. 10 Dimensionless plots of true, model, and assimilated solutions. The three different representer solutions correspond to different covariances as described in the text

6 Conclusions

This is the first time the RM has been applied to this simplified two-phase system, also known as the Buckley–Leverett equation. A linearization of the E-L system was proposed and was found to converge, albeit with the modification of each iterate via damping. The quality of the assimilation was analyzed and compared with the ensemble Kalman smoother, especially in regards to the accurate front dynamics. Another example was shown where the RM tried to correct for wrongly specified permeabilities. It was shown that the covariances were important to the quality of the assimilation.

A natural next step is the extension of this research to the parameter estimation problem, where the goal is recovering better estimates of the parameters governing the system [12]. There has been much work in the subsurface community to estimate permeabilities using a variety of techniques involving Gauss–Newton or gradient-based searches [18]. Reid presents a Gauss–Newton search for the parameters in a subsurface contamination problem that is optimized by using the representers as a basis [23]. The inverse problem using the full RM for reservoirs has been studied by Rommelse et al. and by Przybysz-Jarnut et al. [21, 24]. The latter also compared the RM to the ensemble Kalman filter. There are also some interesting results for other systems [9, 10]. In addition, the EnKF has been used to estimate near-well parameters in the subsurface and model parameters in a two-phase bubble flow [17, 19, 20].

Another important question that can be addressed is over the existence and uniqueness of the minimizer for the cost functional of the nonlinear two-phase model. There may be multiple minima, in which case, it must be asked whether the solution given by the RM is a local minimum or also the global minimum [15]. Though for the specific cases tried in this work, the RM converged to a solution that reduced the value of the cost functional, it is not clear whether that solution is a global or even a local minimum.

The linearization used for the two-phase flow is rather simple and suffered from the need to dampen iterates. The nonlinear flux term was approximated by

$$\left(f\left(S_{\mathrm{w}}^{n}\right)\right)_{x} = f'\left(S_{\mathrm{w}}^{n}\right)\left(S_{\mathrm{w}}^{n}\right)_{x} \approx f'\left(S_{\mathrm{w}}^{n-1}\right)\left(S_{\mathrm{w}}^{n}\right)_{x}.$$

It would be fruitful to look at some other linearizations that may be more stable and converge faster. One that may meet with success, though at the expense of adding an extra term, is

$$f'\left(S_{\mathrm{w}}^{n}\right)\left(S_{\mathrm{w}}^{n}\right)_{x} \approx \left(f'\left(S_{\mathrm{w}}^{n-1}\right) + \left(S_{\mathrm{w}}^{n} - S_{\mathrm{w}}^{n-1}\right) f''\left(S_{\mathrm{w}}^{n-1}\right)\right)\left(S_{\mathrm{w}}^{n}\right)_{x}.$$

While the two-phase flow model presented is useful in certain limited situations, the ultimate goal for practical data assimilation is running the algorithms on more complicated subsurface models that are in use every day. In particular, one would like to see the RM applied to a three-phase, multi-component system in three-dimensional, with features such as wells and faults fully realized. The biggest hurdle, and the biggest drawback of the RM, is deriving and coding the adjoint solver and the linearized forward solver for the representers.

A real-world application should also be cycling, in the sense that the covariances are updated at the end of the assimilation in preparation for a new cycle. The RM as derived does not update the statistics; however, Xu and Daley show how this can be done consistently at the cost of calculating a representer for each grid point [26]. This is too burdensome computationally. Therefore, it would be useful to study ways of simplifying their scheme so that the RM cycles competitively with Kalman filter variants.

References

1. Ababou, R., McLaughlin, D., Gelhar, L.W., Tompson, A.F.B.: Numerical simulation of three-dimensional saturated flow in randomly heterogeneous porous media. Trans. Porous Media **4**, 549–565 (1989)
2. Baird, J., Dawson, C.: A posteriori error estimation of the representer method for single-phase Darcy flow. ICES Report 05-43, 1–16 (2005)
3. Baird, J., Dawson, C.: The representer method for data assimilation in single-phase Darcy flow in porous media. Comput. Geosci. **9**, 247–271 (2005)
4. Bear, J.: Dynamics of Fluids in Porous Media. Dover, New York (1988)
5. Bennett, A.F.: Inverse methods in Physical Oceanography. Cambridge University Press, New York (1992)
6. Bennett, A.F.: Inverse Modeling of the Ocean and Atmosphere. Cambridge University Press, Cambridge (2002)
7. Burgers, G., van Leeuwen, P.J., Evensen, G.: Analysis scheme in the ensemble Kalman filter. Mon. Weather Rev. **126**, 1719–1724 (1998)
8. Dawson, C.N.: Godunov-mixed methods for immiscible displacement. Int. J. Numer. Methods Fluids **11**, 835–847 (1990)
9. Eknes, M., Evensen, G.: Parameter estimation solving a weak constraint variational formulation for an Ekman model. J. Geophys. Res. **102**, 12479–12491 (1997)
10. Evensen, G.: Advanced data assimilation for strongly nonlinear dynamics. Mon. Weather Rev. **125**, 1342–1354 (1996)
11. Evensen, G.: The ensemble Kalman filter: theoretical formulation and practical implementation. Ocean Dyn. **53**, 343–367 (2003)
12. Ewing, R.E., Pilant, M.S., Wade, J.G., Watson, A.T.: Estimating parameters in scientific computation: A survey of experience from oil and groundwater modeling. IEEE Comput. Sci. Eng. **1**, 19–31 (1994)
13. Freeze, R.A., Cherry, J.A.: Groundwater. Prentice-Hall, Englewood Cliffs (1979)

14. Godunov, S.K.: A finite difference method for the numerical computation and discontinuous solutions of the equations of fluid dynamics. Mat. Sb. **47**, 271 (1959)
15. Hagelberg, C.R., Bennett, A.F., Jones, D.A.: Local existence results for the generalized inverse of the vorticity equation in the plane. Inverse Problems **12**, 437–454 (1996)
16. LeVeque, R.J.: Numerical Methods for Conservation Laws. Birkhäuser Verlag, Berlin (1992)
17. Lorentzen, R.J., Nævdal, G., M Lage, A.C.V.: Tuning of parameters in a two-phase model using an ensemble Kalman filter. Int. J. Multiph. Flow **29**, 1283–1309 (2003)
18. McLaughlin, D., Townley, L.R.: A reassessment of the groundwater inverse problem. Water Resour. Res. **32**, 1131–1161 (1996)
19. Nævdal, G., Johnsen, L.M., Aanonsen, S.I., Vefring, E.H.: Reservoir monitoring and continuous model updating using ensemble Kalman filter. Paper SPE 84372, presented at the SPE Annual Technical Conference and Exhibition held in Denver, Colorado (2003)
20. Nævdal, G., Mannseth, T., Vefring, E.H.: Near-well reservoir monitoring through ensemble Kalman filter, Paper SPE 75235, presented at the SPE/DOE Improved Oil Recovery Symposium held in Tulsa, Oklahoma (2002)
21. Przybysz-Jarnut, J.K., Hanea, R.G., Jansen, J.D., Heemink, A.W.: Application of the representer method for parameter estimation in numerical reservoir models. Comput. Geosci. **11**, 73–85 (2007)
22. Reichle, R.H., McLaughlin, D.B., Entekhabi, D.: Hydrologic data assimilation with the ensemble Kalman filter. Mon. Weather Rev. **130**, 103–114 (2002)
23. Reid, L.B.: A functional inverse approach for three-dimensional characterization of subsurface contamination. Ph.D. dissertation, Massachusetts Institute of Technology (1996)
24. Rommelse, J.R., Kleptsova, O., Jansen, J.D., Heemink, A.W.: Data assimilation in reservoir management using the representer method and the ensemble Kalman filter, Proceedings of the 10th European Conference on the Mathematics of Oil Recovery—ECMOR X (2006)
25. Valstar, J.R.: Inverse modeling of groundwater flow and transport. Ph.D. dissertation, Technische Universiteit Delft (May 2001)
26. Xu, L., Daley, R.: Towards a true 4-dimensional data assimilation algorithm: application of a cycling representer algorithm to a simple transport problem. Tellus **52A**, 109–128 (2000)